



US Army Corps
of Engineers®

ERDC TN-EQT-13-1
September 2013

Modeling RDX Reduction within Iron Bed Reactors

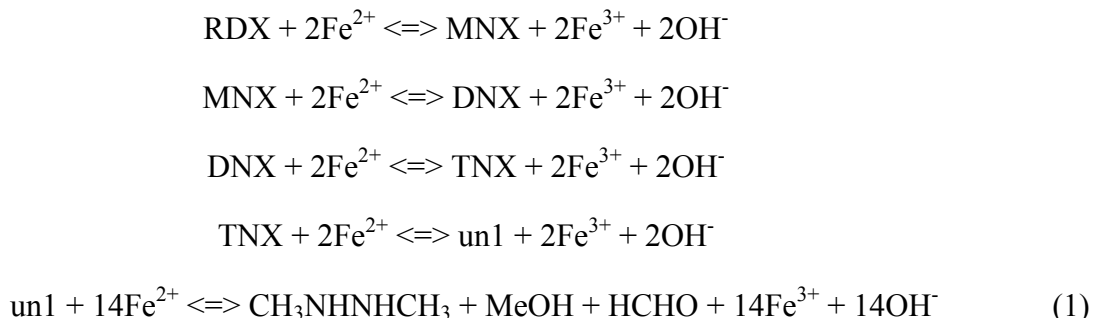
by Mark S. Dortch and Heather M. Smith

PURPOSE: Iron has been used to reduce organic contaminants including high explosives (HE) such as Research Department Explosive (RDX). Work is ongoing at the U.S. Army Engineer Research and Development Center (ERDC) to develop guidelines for using iron bed reactors to remove RDX in surface water runoff from the impact areas of firing ranges. As part of this work, a mathematical model was developed to gain a better understanding of the experimental results and to provide information for design and operation of these reactors. This model and its application results are described within this technical note (TN).

Following additional validation against field data, this model will be implemented within the Training Range Environmental Evaluation and Characterization System (TREECS™) (<http://el.erd.c.usace.army.mil/treecs/>). TREECS™ was developed by ERDC for the Army with varying levels of capability to forecast the fate of munitions constituents (MC), such as HE and metals, within and transported from firing/training ranges to surface water and groundwater. The overall purpose of TREECS™ is to provide environmental specialists with tools to assess the potential for MC migration into surface water and groundwater systems and to assess range management strategies to ensure protection of human health and the environment. Although TREECS™ was developed to forecast the fate of MC on firing ranges, it has general applicability to many other situations requiring prediction of contaminant fate in multi-media environmental systems.

BACKGROUND: Munitions containing HE fired into impact areas can infrequently experience low-order detonations that result in unexploded MC residue. MC residues that build up over time can be transported with water to off-range receiving water, potentially resulting in concentrations exceeding protective health guidelines. Methods are sought that can be implemented in the field to remove RDX in runoff from firing range impact areas. Metallic iron can be mixed with other materials, such as gravel, biodegradable organic matter, and iron-reducing bacteria, to create a reactor bed for reducing RDX and its degradation products. For field conditions, the reactor can be placed within a trench that collects rainfall runoff from the firing range impact area. The reactor is water-saturated, which, in the presence of oxygen, causes the metallic iron to rust forming Fe(II) and Fe(III). Acetate is added to the reactor providing food substrate for the bacteria. As the substrate is utilized by the bacteria, oxygen and Fe(III) serve as electron acceptors, thus reducing most of the iron to Fe(II). When RDX is introduced into the reactor, Fe(II) serves as an electron donor, and RDX serves as the electron acceptor, thus oxidizing Fe(II) to Fe(III) while reducing RDX through the sequence of degradation products of MNX, DNX, TNX, and eventually various end-products, such as formaldehyde. If RDX is continually supplied to the reactor, much of the Fe(II) can be converted to Fe(III), and the reactor loses its ability to degrade RDX. Thus, acetate must be re-supplied to reduce Fe(III) to Fe(II). Additionally, some of the Fe(II) can become dissolved and flushed out by the water flowing through the reactor.

A degradation pathway for RDX is shown in Figure 1. Two electrons are required for each degradation step. The proposed reactions (Szecsody et al. 2001) in these degradation processes are:



where *unl* is a non-cyclic unknown compound that degrades into benign by-products. ShROUT et al. (2004) suggest that *unl* is three moles of hydroxymethylnitrosamine following hydrolysis.

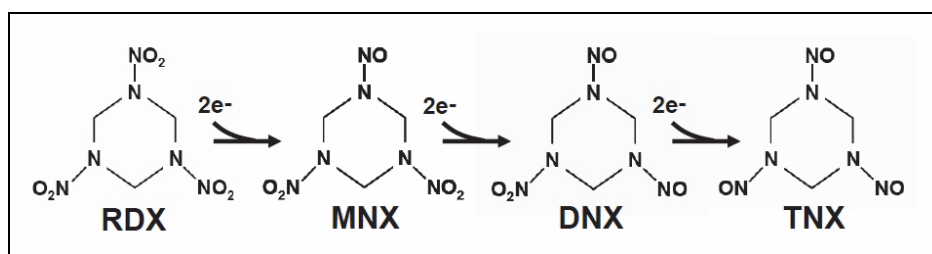


Figure 1. Proposed degradation pathway for RDX and metabolites.

A study by Wanaratna et al. (2006) clearly indicates that their observed RDX degradation rates were dependent upon the amount of solid phase, zero-valent iron (ZVI) within their reactor, and their results support the theory that the reduction of RDX occurs on the surfaces of the solid iron. These results are important since they indicate that the model development should proceed along the path of surface site reaction following mass transfer of dissolved RDX from pore-water to solid surfaces. This modeling approach is quite different from an approach representing reactions of dissolved RDX and iron in water.

OBJECTIVE: The objective of this study was to develop a model to predict the degradation of RDX and its degradation products within an iron bed reactor. A batch reactor model and a one-dimensional (1D), longitudinal reactor model are derived for surface site reactions and tested against laboratory experiments as described below.

MODEL FORMULATION FOR BATCH REACTOR: Mass balance equations with first-order degradation kinetics can be used to model the concentrations of RDX and its degradation products shown in Equation set 1. These equations are first developed for a single fully mixed (batch) reactor consisting of a water-saturated porous media, with a constant RDX loading, and for a constant water flow rate through the reactor. These equations are stated as follows:

$$\frac{d \text{RDX}}{dt} = \frac{\text{RDX}_{in} Q}{\phi V_T} - \frac{\text{RDX} Q}{\phi V_T} - k_1 \text{RDX} \quad (2)$$

$$\frac{d\text{MNX}}{dt} = k_1 \text{RDX} - \frac{\text{MNX} Q}{\phi V_T} - k_2 \text{MNX} \quad (3)$$

$$\frac{d\text{DNX}}{dt} = k_2 \text{MNX} - \frac{\text{DNX} Q}{\phi V_T} - k_3 \text{DNX} \quad (4)$$

$$\frac{d\text{TNX}}{dt} = k_3 \text{DNX} - \frac{\text{TNX} Q}{\phi V_T} - k_4 \text{TNX} \quad (5)$$

$$\frac{d\text{un1}}{dt} = k_4 \text{TNX} - \frac{\text{un1} Q}{\phi V_T} - k_5 \text{un1} \quad (6)$$

where

$k_{1,2,3,4,5}$ = overall degradation rates including mass transfer to surface sites and surface site reaction rate, hr^{-1}

RDX_{in} = concentration of RDX flowing into the reactor, mg/L

Q = flow rate of water through the reactor and carrying RDX into the reactor, L/hr

t = time, hr

ϕ = porosity of the reactor media, water volume/total volume

V_T = reactor total volume, liters (L)

Concentrations of all constituents (RDX, MNX, etc.) are expressed in mg/L . The product $\text{RDX}_{in}Q$ is the RDX loading rate (mg/hr) into the reactor. It is assumed that all constituents (RDX and degradation products) are dissolved in water (i.e., mass/volume water) and that sorption partitioning is minor and can be ignored. This last assumption is reasonable given the range of partitioning coefficients for RDX and its degradation products. It is assumed for this model that the concentration of Fe(II) is plentiful and continuous over time, which means that acetate or a similar food source for reducing bacteria is regularly provided to the reactor. Therefore, this model does not attempt to compute the supply or concentration of Fe(II).

For this model development, it is assumed that all of the RDX degradation products have the same reaction rate as RDX, i.e., $k_1=k_2=k_3=k_4=k_5=k$. As mentioned above, the reaction rate k (hr^{-1}) is an overall reaction rate that accounts for mass transfer from pore water to solid surfaces and surface-site reaction (i.e., reduction). The immediate goal is to derive a relationship for determining k .

Mass transfer here refers to the movement of solute (e.g., RDX) from pore water to solid surface (iron). For a general solute concentration C (mg/L), this mass transfer can be described as follows:

$$\frac{dC}{dt} = -k_m a_s (C - C_b) \quad (7)$$

where

k_m = the mass transfer coefficient, m/hr^{-1}

a_s = specific surface area of solids, which is the solid surface area a divided by the pore-water volume V_w , m^{-1}
 C_b = solute concentration at the solid surface, mg/L

The problem with Equation 7 is that the parameters k_m , a_s , and C_b are difficult to determine. To simplify matters, the product of the first two parameters can be represented by the mass transfer rate λ (per hour), or

$$\frac{dC}{dt} = -\lambda(C - C_b) \quad (8)$$

An approach for estimating λ is presented later below.

The solute concentration at the surface of the solid C_b is driven by the surface-site reaction

$$\frac{dC_b}{dt} = -KC_b \quad (9)$$

where K is the surface-site reaction rate (per time). Wanaratna et al. (2006) tested RDX reduction using zero-valent iron (ZVI) and determined that K is related to the amount of ZVI through a Monod relationship

$$K = \frac{k_{max} [ZVI]}{k_0 + [ZVI]} \quad (10)$$

with $k_{max} = 2.824 \text{ min}^{-1}$ or 0.047 sec^{-1} , and $k_0 = 1.806 \text{ M (mole/L)}$. The concentration of ZVI is also in moles/L and can be determined by dividing the total mass (g) of ZVI in the reactor by the reactor water volume (ϕV_T) and dividing the result by the molecular weight of iron (55.85 g/mole). For the present reactor conditions, it is the concentration [Fe(II)] that is required in Equation 10 rather than [ZVI]. Thus, the values for k_{max} and k_0 in Equation 10 could be different for Fe(II) than for ZVI. If the concentration of Fe(II) is much greater than the half-saturation concentration for Fe(II), i.e., k_0 , then K is simply equal to k_{max} .

Considering that equilibrium conditions should eventually exist between mass transfer and surface-site reaction, Equations 8 and 9 can be set equal to each other, resulting in

$$\lambda(C - C_b) = KC_b \quad (11)$$

or

$$C_b = \frac{\lambda C}{\lambda + K} \quad (12)$$

Substituting the above relation for C_b into Equation 8 yields

$$\frac{dC}{dt} = -\left(\frac{\lambda K}{\lambda + K}\right)C = -kC \quad (13)$$

Thus, the overall reaction rate k accounting for mass transfer and surface-site reaction is

$$k = \frac{\lambda K}{\lambda + K} \quad (14)$$

When K is large compared to λ , the overall reaction rate is driven by mass transfer. When λ is large compared to K , the overall reaction rate is driven by the surface-site reaction rate.

Mass transfer between fluid and liquid and fluid and solid has been extensively studied over the past 50 years. Many such studies involved dissolving spheres or cylinders in packed beds or suspended in fluids. Although various correlations have been used to describe theory and experimental results, there is no one single correlation that seems to work for all conditions. Most of the correlations relate the Sherwood number (Sh) to the Peclet number (Pe).

Many such correlations were reviewed and tested against the meso-scale laboratory results described below in this TN. The one correlation that appeared to hold the most promise is based on data presented by Miyauchi (1971). Figure 6 within the paper by Miyauchi (1971) shows a strong relationship between Sh and Pe , where Sh is defined as $k_m d_p / D_e$ and k_m is the mass transfer coefficient (m/sec); d_p is the diameter (m) of the packed bed material; and D_e is the effective diffusivity (m²/sec) of the solute in fluid within the pore spaces. The Peclet number is defined as $u d_p / D_e$, where u is the pore velocity (m/sec). The pore velocity is the Darcy velocity U divided by the bed porosity, and the Darcy velocity is the reactor water flow rate divided by the cross-sectional area of the flow. For practical purposes, it is assumed that D_e is equivalent to the molecular diffusivity D_m . An approximate fit of the data presented in Figure 6 of Miyauchi (1971) resulted in the relationship

$$Sh = 4Pe^{1/3} \quad (15)$$

Similar relationships have been reported by others, including one documented by Wilson and Geankoplis (1966), which was derived from the dissolution of solid benzoic acid spheres. This relationship was also used successfully by Geller and Hunt (1993) to predict the mass transfer from non-aqueous phase organic liquids to water in porous media. However, the relationship described by Wilson and Geankoplis (1966) was not developed for dilute beds and under-predicted the meso-scale results. Miyauchi (1971) presented data for dilute beds, where the reactive particles were rather sparse relative to the packing particles. This is the situation for solid iron placed in gravel beds, which is the case for the meso-scale experiments and will most likely be the case for field-scale reactors.

Substituting definitions for Sh and Pe , Equation 15 can be solved for k_m

$$k_m = \frac{4u^{1/3} D_m^{2/3}}{d_p^{2/3}} \quad (16)$$

Assuming that the packing particles are spherical, a relationship for specific surface area a_s can be derived from the relationships for the surface area (a) of an individual particle and volume of water (V_w) along with the definition of void fraction or porosity. This relationship is

$$a_s = \frac{a}{V_w} = \frac{6(1-\phi)}{d_p \phi} \quad (17)$$

where ϕ is the porosity as before. Similarly, a relationship for cylindrical packing particles can be derived

$$a_s = \frac{2(1-\phi)}{d_p \phi} \left(\frac{d_p}{l} + 2 \right) \quad (18)$$

where d_p is the diameter (m) of an individual cylindrical particle, and l is its length (m). However, in most cases, it can be assumed that the packing particles are spherical. The mass transfer rate λ (sec^{-1}) for spherical packing particles can now be obtained

$$\lambda = k_m a_s = \frac{24u^{1/3} D_m^{2/3} (1-\phi)}{\phi d_p^{5/3}} \quad (19)$$

For cylindrical packing particles, the mass transfer rate is

$$\lambda = k_m a_s = \frac{8u^{1/3} D_m^{2/3} (1-\phi)}{\phi d_p^{5/3}} \left(\frac{d_p}{l} + 2 \right) \quad (20)$$

When the cylinder length is equal to the cylinder diameter, Equation 20 becomes the same as Equation 19.

It is necessary to allow for a minimum mass transfer rate for no flow or stagnant pore-water conditions. Even under stagnant conditions, there will be some solute movement due to molecular diffusion. The literature, including Miyauchi (1971), consistently indicated that a minimum Sh of approximately 2.0 describes mass transfer when $Pe \ll 1$, or when there is essentially no flow. Thus, $Sh = 2$ was used for setting a minimum mass transfer rate, resulting in the following relationship for spherical packing particles:

$$\lambda_{\min} = \frac{12 D_m (1-\phi)}{\phi d_p^2} \quad (21)$$

The minimum mass transfer rate for cylindrical packing particles is

$$\lambda_{\min} = \frac{4 D_m (1-\phi)}{\phi d_p^2} \left(\frac{d_p}{l} + 2 \right) \quad (22)$$

Using either Equation 19 or 20 (with Equations 21 and 22 for lower limits) and an estimate of K from Equation 10, k can be obtained from Equation 14, and Equations 2–6 can be solved for RDX and its degradation products. It is assumed that at time zero, the RDX concentration in the reactor is known, and the initial concentrations of MNX, DNX, TNX, and un1 are zero. The flow rate and RDX concentration of water entering the reactor are also known, as well as the mass of iron in the reactor, which is assumed to be Fe(II). With the input parameters, initial conditions, and boundary conditions, the five differential equations are solved in a spreadsheet yielding the constituent concentration over time, where the time-step of the solution is specified by the user. The first-order-accurate, Euler integration method is used for the solution.

A conservative tracer is also included within the model to evaluate flushing time. The mass balance equation for a tracer moving through the fully mixed reactor is

$$\frac{dC}{dt} = \frac{Q}{\phi V_T} (C_{in} - C) \quad (23)$$

where C is the tracer concentration in the reactor, and C_{in} is the tracer concentration in the inflow.

SOLUTIONS WITH BATCH REACTOR MODEL: The batch reactor model was first applied to a hypothetical reactor for several conditions to gain an understanding of basic model behavior. The first test case consisted of no water flow and no RDX loading into the reactor but with an initial RDX concentration within the reactor. Reactor input conditions are shown in Table 1. The two reaction kinetic parameters were set to those determined for ZVI by Wanaratna et al. (2006) pending availability of additional data for Fe(II) as the reactant.

Input Parameter	Input Value	Units
Reactor volume, V_T	100	L
Media porosity, ϕ	0.5	dimensionless
Water flow rate entering/exiting, Q	0	L/hr
RDX concentration flowing in, RDX_{in}	0	mg/L
Initial RDX concentration in reactor	1.0	mg/L
Mass of iron in the reactor	1000	g
Average particle diameter of packed bed material, d_p	.01	m
Molecular diffusivity of RDX and degradation products, D_m	5.9E-10	m ² /sec
Maximum surface site reaction rate, k_{max}	2.824	min ⁻¹
Half-saturation concentration of iron for surface site reaction, k_0	1.806	mole/L

The time series results for this test case are shown in Figure 2 for RDX and its degradation products. Since there is no loading of RDX after the initial specified concentration, the RDX concentration drops over time. The degradation products build up and then die off over time in the sequence of the pathway shown in Figure 1.

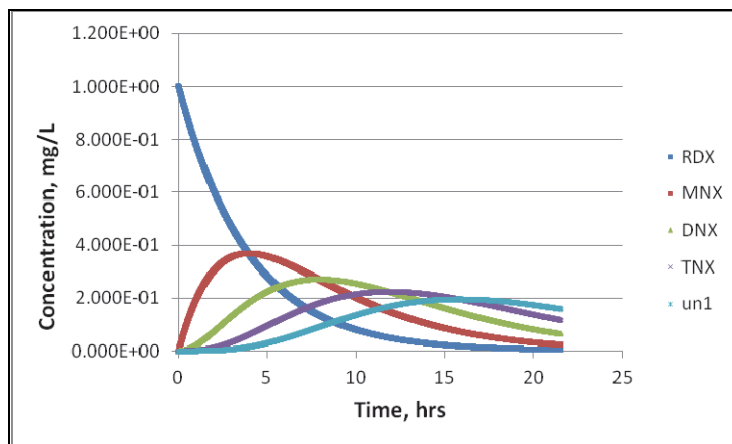


Figure 2. Concentrations of RDX and degradation products versus time for hypothetical batch reactor, first test case.

The second test for the hypothetical reactor was for a constant water flow rate of 10 L/hr, but with zero RDX in the inflow. All other inputs remained the same as the first test case, which included an initial RDX concentration of 1.0 mg/L. The inputs for this test condition are shown in Table 2.

Table 2. Input parameters for hypothetical batch reactor model, second test case.		
Input Parameter	Input Value	Units
Reactor volume, V_T	100	L
Media porosity, ϕ	0.5	dimensionless
Water flow rate entering/exiting, Q	10	L/hr
RDX concentration flowing in, RDX_{in}	0	mg/L
Initial RDX concentration in reactor	1.0	mg/L
Mass of iron in the reactor	1000	g
Average particle diameter of packed bed material, d_p	.01	m
Molecular diffusivity of RDX and degradation products, D_m	5.9E-10	m ² /sec
Maximum surface site reaction rate, k_{max}	2.824	min ⁻¹
Half-saturation concentration of iron for surface site reaction, k_0	1.806	mole/L

The results of the second test are shown in Figure 3 for RDX and its degradation products. These results are similar to those of the first test case, except that the decline of concentrations is faster due to flushing with clean water. A tracer concentration of 100 mg/L was introduced within the reactor influent. The tracer concentration versus time for the second test is shown in Figure 4. The tracer approaches the inflowing tracer concentration of 100 mg/L as time progresses. The hydraulic residence time of the reactor is 5 hr; thus, it takes longer than this for the reactor to reach the steady-state concentration of 100 mg/L. The tracer results agree with analytical results for this test case, such as requiring 11.5 hr to reach a level of 90% completely flushed.

The third test case for the hypothetical batch reactor was conducted with a constant RDX loading as prescribed for a water flow rate of 10 L/hr with an RDX concentration of 1.0 mg/L in this flow. The initial RDX concentration in the reactor was set to zero. All other inputs were the same as for the first

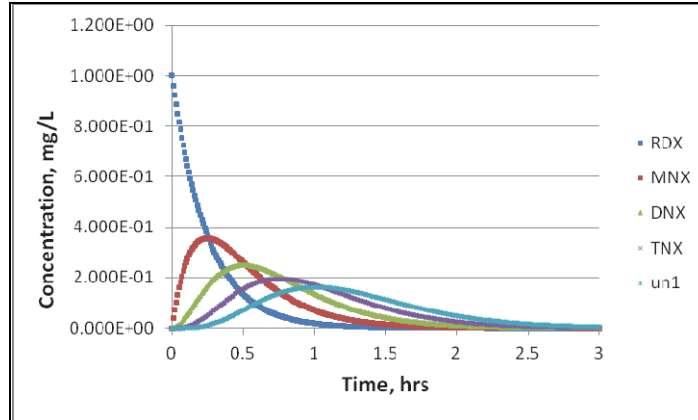


Figure 3. Concentrations of RDX and degradation products versus time for hypothetical batch reactor, second test case.

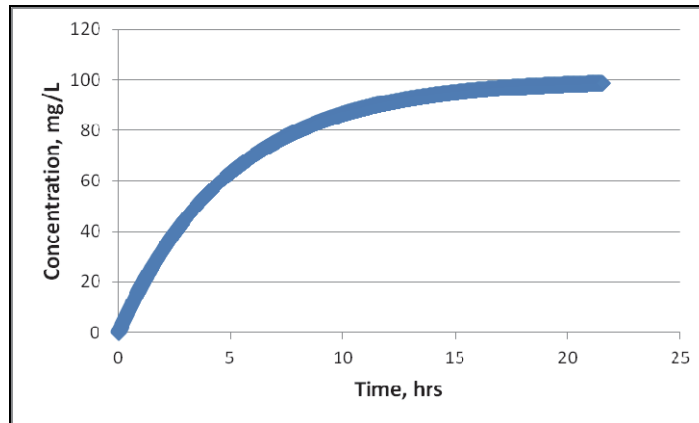


Figure 4. Tracer concentration versus time for hypothetical batch reactor, second test case.

Table 3. Input parameters for hypothetical batch reactor model, third test case.		
Input Parameter	Input Value	Units
Reactor volume, V_T	100	L
Media porosity, ϕ	0.5	dimensionless
Water flow rate entering/exiting, Q	10	L/hr
RDX concentration flowing in, RDX_{in}	1.0	mg/L
Initial RDX concentration in reactor	0	mg/L
Mass of iron in the reactor	1000	g
Average particle diameter of packed bed material, d_p	.01	m
Molecular diffusivity of RDX and degradation products, D_m	5.9E-10	m ² /sec
Maximum surface site reaction rate, k_{max}	2.824	min ⁻¹
Half-saturation concentration of iron for surface site reaction, k_0	1.806	mole/L

two tests. The inputs for this test case are shown in Table 3. The results of this test case are shown in Figure 5. RDX reaches a steady-state concentration balanced by losses due to degradation and flushing and gains due to the constant loading of RDX. Likewise, constant concentrations of RDX degradation products are produced. The results for all three of the hypothetical batch reactor tests appear to be reasonable and expected.

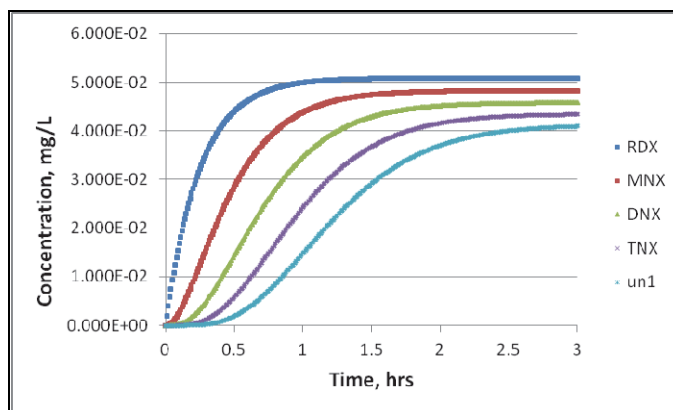


Figure 5. Concentrations of RDX and degradation products versus time for hypothetical batch reactor, third test case.

The batch reactor model was next applied to laboratory tests conducted in the ERDC Environmental Laboratory. These tests were conducted with 100-mL vials containing iron filings and spiked with soil as inoculants and an initial dissolved RDX concentration of 4.0 mg/L. A metallic iron mass of 0.02 g was added to the vials initially. Thus, each vial contained 3.58 mmol/L of iron. The RDX concentration in the vials was measured over 60 days. Tests were conducted at 30 and 13.5 °C in MaxQ 6000 Incubated/Refrigerated Shakers (Thermo Scientific, USA). The measured RDX concentrations decreased with increasing time, but there was little difference in results for the two temperature conditions. Therefore, the observed concentrations for the two temperatures were averaged for each sampling time point. The vials were shaken continuously at 130 RPM during the experiment. The iron filings were approximately 0.5 mm wide and 1 mm long. Thus, the filings were assumed to be cylindrical.

The porosity was computed from

$$\phi = 1 - \frac{V_s}{V_T} = 1 - \frac{M_s}{\rho_s V_T} \quad (24)$$

where V_s is the volume (m^3) of solid iron, V_T is the reactor volume (m^3), M_s is the mass (g) of solid iron in the system, and ρ_s is the density of solid iron of $7.87E6 \text{ g/m}^3$. It is not known how fast the water was moving within the vials when shaken, so u (pore velocity) was varied until model results matched observed data. Using a value of zero for u resulted in insufficient RDX reduction over time. The calibrated value of u was $1.0E-5 \text{ m/sec}$. The values for the two kinetic parameters were set to the values used for the previous tests. All input values for this test case are summarized in Table 4.

Table 4. Input parameters for batch reactor model, laboratory experiment with 100-mL vial.		
Input Parameter	Input Value	Units
Reactor volume, V_T	0.1	L
Media porosity, ϕ	0.999975	dimensionless
Water flow rate entering/exiting, Q	0	L/hr
RDX concentration flowing in, RDX_{in}	0	mg/L
Initial RDX concentration in reactor	4	mg/L
Mass of iron in the reactor	0.02	g
Average particle diameter of packed bed material, d_p	.0005	m
Average particle length of packed bed material, l	.001	m
Molecular diffusivity of RDX and degradation products, D_m	5.9E-10	m ² /sec
Maximum surface site reaction rate, k_{max}	2.824	min ⁻¹
Half-saturation concentration of iron for surface site reaction, k_o	1.806	mole/L
Calibrated u	1.0E-5	m/sec

Observed and model-computed RDX concentrations for the vial experiment are compared in Figure 6. The model matches the observed data closely, but it was necessary to adjust u to reach such agreement since the value of this variable was not known for shaken vials. A greater value of u causes under-prediction of concentration, and a smaller value causes over-prediction. This application was not an adequate validation of the model due to the need to adjust u .

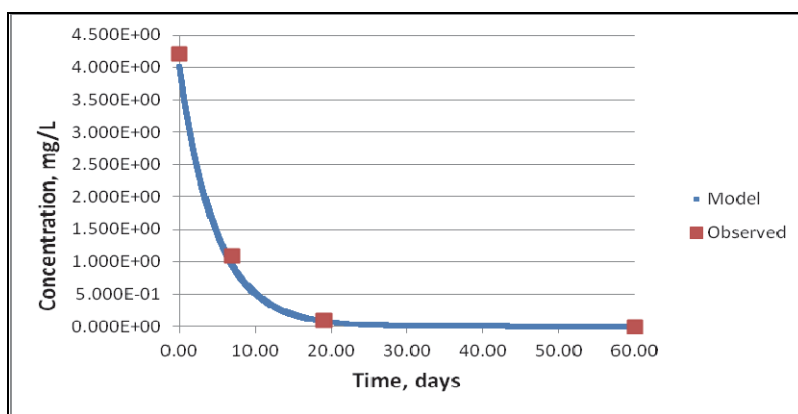


Figure 6. RDX concentration versus time for laboratory vial experiment.

MODEL FORMULATION FOR 1D LONGITUDINAL REACTOR: This model is designed to account for constituent variations along the longitudinal axis of the reactor as well as transport through the mobile domain and constituent storage in the immobile domain. Consider a water-saturated, longitudinal reactor of uniform width, depth, and porous media properties (e.g., porosity ϕ) that receives a water flow rate and loading of RDX at the upstream end. For a given water inflow rate Q (L/hr), reactor width W (m), and depth H (m), the Darcy velocity U (m/hr) through the reactor can be computed from $U = \frac{Q}{1000WH}$. Dispersion can also be included in the transport along the

reactor. Transport trapping is included through the use of a dual-domain modeling approach (Zheng and Wang 1999, Liu et al. 2007). Dual-domain models provide a means to represent the effects of dead-end pores. The time-varying, one-dimensional reactive transport equation for the longitudinal reactor for mobile and immobile solute constituent concentrations is

$$\frac{\partial C_m}{\partial t} = \frac{\zeta}{f\phi}(C_{im} - C_m) + D_x \frac{\partial^2 C_m}{\partial x^2} - \frac{U}{f\phi} \frac{\partial C_m}{\partial x} - k C_m + S_m \quad (25)$$

$$\frac{\partial C_{im}}{\partial t} = \frac{\zeta}{(1-f)\phi}(C_m - C_{im}) - k_{min} C_{im} + S_{im} \quad (26)$$

where

C_m = solute concentration in the mobile domain (mg/L)

C_{im} = solute concentration in the immobile domain (mg/L)

f = fraction of domain that is mobile or ϕ_m/ϕ where ϕ_m is the mobile or effective porosity

x = distance along the longitudinal axis of the reactor (m)

t = time (hr)

D_x = dispersion coefficient (m²/hr)

k = overall reaction rate in the mobile domain accounting for mass transfer and surface-site reaction (1/hr)

k_{min} = the minimum overall reaction rate accounting for mass transfer and surface-site reaction for no flow in the immobile domain (1/hr), $k_{min} = \frac{\lambda_{min} K}{\lambda_{min} + K}$

U = Darcy velocity (m/hr)

ϕ = bed porosity (dimensionless)

S_m = source term in the mobile domain (mg/L/hr)

S_{im} = source term in the immobile domain (mg/L/hr)

ζ = first-order mass transfer rate between mobile and immobile domains (1/hr)

The variable k is the same as previously defined for the batch reactor. It is noted that the two above equations do not include sorption partitioning; thus, the solute is assumed to have a very low partitioning coefficient, which is generally the case for RDX and its degradation products.

The source terms S_m and S_{im} are zero for RDX. The source term for MNX is the kinetic loss term for RDX, or

$$S_m(MNX_m) = \frac{\lambda K}{\lambda + K} RDX_m \quad (27)$$

$$S_{im}(MNX_{im}) = \frac{\lambda_{min}K}{\lambda_{min} + K} RDX_{im} \quad (28)$$

Likewise, the source term for DNX is the kinetic loss term for MNX, and so on down the reaction chain. This model only allows for spherical bed solids. The mass transfer rate for the mobile domain is set to the maximum value of λ computed from Equation 19 and λ_{min} computed from Equation 21, thus allowing for cases when the flow velocity is small. The mass transfer rate for the immobile domain is λ_{min} as determined from Equation 21.

Dispersivity is used within the model to compute the spatially varying, longitudinal dispersion coefficient as follows:

$$D_x = \alpha_x XU \quad (29)$$

where $\alpha_x X$ is the longitudinal dispersivity, α_x is the proportionality constant (dimensionless), and X is the distance from the beginning of the reactor (where water flows in) to the location of interest. A typical, commonly used value of the longitudinal dispersivity constant is 0.1.

Equations 25 and 26 include two unknowns (C_m and C_{im}) that must be numerically solved over the two independent variables x and t , the space and time domains. The initial conditions for this model are zero concentration for all constituents. The boundary conditions that are specified at $x = 0$ are zero concentration for all constituents except for RDX, which is specified. The flow rate of water entering the reactor, and thus the flow speed, as well as the concentration of RDX in the influent water, can be varied over time for this more general-purpose model. However, this added flexibility requires a numerical solution that is better suited to programming with a computer coding language.

The above formulations were programmed into a numerical model code using Fortran. The finite difference method was used to discretize time and space and solve the two partial differential equations. The equations are solved explicitly using a forward difference in time and options of either central or upwind differencing for advection (the third term on the right-hand side of Equation 25). A central difference was used for the dispersion term (the second term on the right-hand side of Equation 25). The model code checks for numerical stability requirements associated with the solution schemes. It is noted that the dispersion term cannot be zero if stability is to be maintained when using the central difference for advection.

SOLUTIONS WITH THE 1D LONGITUDINAL REACTOR MODEL: Hypothetical reactor conditions closely similar to the third test conditions described in the batch reactor model applications were applied to the longitudinal reactor model. These test conditions are shown in Figure 7. The length of the reactor was set to 1.0 m, and the width and height were set to 0.32 m, which yielded approximately the same total volume of 100 L as used for the batch reactor test case. The fraction of mobile domain was set to 1.0.

Most of the inputs shown in Figure 7 are self-explanatory, but a few require further definition. The input variable labeled “domain mass trans rate” is ζ and is shown in Equations 25 and 26. The variable “number of delta x” is the number of computational segments NX that the total reactor length is to be discretized. For the example shown, $NX=10$; thus, the spatial size of each computational segment is 0.1 m. The variable “DX output intervals” prescribes the number of segments to skip within the

discretized X space for writing output. For example, a value of 2 means that output will be written for every second segment, starting with segment 1 and ending at the last segment. The variable “solution scheme” should have a value of either 0 or 1. A value of 0 denotes that the upwind differencing scheme is used for advection, whereas a value of 1 denotes that the central differencing scheme is used.

As with the batch reactor model, two iron kinetic reaction parameters must be specified, potentially requiring calibration against laboratory or field results. The default values are shown in Figure 7. Two additional parameters (f and ζ) are introduced by using the dual-domain modeling approach to account for transport trapping. Additionally, the longitudinal dispersivity constant must be specified, but the default value shown in Figure 7 is typically used. The time-step and number of spatial segments may have to be adjusted to provide numerical stability and sufficient accuracy.

"Test case for generic 1D reactor model"				
"Length, m"				1.0
"Width, m"				.32
"Height, m"				.32
"Porosity"				0.50
"fraction mobile"				1.0
"Dispersivity constant"				0.1
"domain mass trans rate, 1/hr"				1.0
"RDX mole. diffus., cm2/sec"				5.9E-6
"packing solids diam, m"				.01
"Fe mass in reactor, kg"				1.
"Fe half sat conc, k0, mol/L"				1.806
"Fe max reac rate, kmax, 1/min"				2.824
"RDX initial, mg/L"				0.0
"number of delta x"				10
"delta t, hr"				.01
"simulation duration, hr"				20.
"DX output intervals"				2
"solution scheme"				1
"Time, hr	flowin, L/hr	RDX in, mg/L	Tracer in, mg/L"	
0.0	10.0	1.0	1.0	
2.0	10.0	1.0	1.0	

Figure 7. Input parameters for longitudinal reactor model, hypothetical test conditions.

The pore water concentrations of RDX and its degradation products in the mobile domain (as computed by the longitudinal reactor model) are plotted versus time in Figure 8 for a location 0.25 m down-gradient of the influent. All concentrations reach steadystate after a few hours. At this location, the reduction of RDX has resulted in a buildup of degradation products that exceed the RDX concentration, which is an inverse relationship compared to the results shown in Figure 5. Thus, a longitudinal reactor can respond quite differently from a batch reactor.

The concentrations versus distance values for this test condition after 20 hr are plotted in Figure 9. This figure shows the rapid loss of RDX followed by the growth of RDX products and their subsequent degradation with distance down-gradient. The cross-over point at which the RDX concentration falls below the product concentrations occurs at approximately $X = 0.2$ m.

The hypothetical longitudinal reactor test case described above was repeated; however, a conservative tracer pulse (as shown in Figure 10) was introduced in the influent to evaluate the effects of including an immobile domain. Additionally, the spatial resolution was doubled using 20 segments rather than

10. Otherwise, the input conditions of Figure 7 were imposed. Three tests were run. The first test was for a 100% mobile domain. The second and third tests were run with a 50% mobile domain for both tests, but with domain mass transfer rates of 1.0/hr and 0.1/hr. The tracer concentration results for the square tracer input pulse are shown in Figure 11. The results for 100% mobile domain demonstrate that roughly a square distribution of tracer concentration versus time occurs at the sampling location ($X = 0.425$ m). There is some longitudinal dispersion in the solution due to the value set for dispersivity as well as due to some numerical diffusion associated with the solution scheme. The results for a 50% mobile domain and a mass transfer rate of 1.0/hr demonstrate a time-delayed and more diffuse tracer distribution. Higher domain mass transfer rates showed little change from this result for these test conditions. The results for a 50% mobile domain and a mass transfer rate of 0.1/hr follow those of the 100% mobile domain initially, but the peak concentration is reached later, and the tailing concentrations recede more gradually. Overall, these test results appear to follow logical considerations.

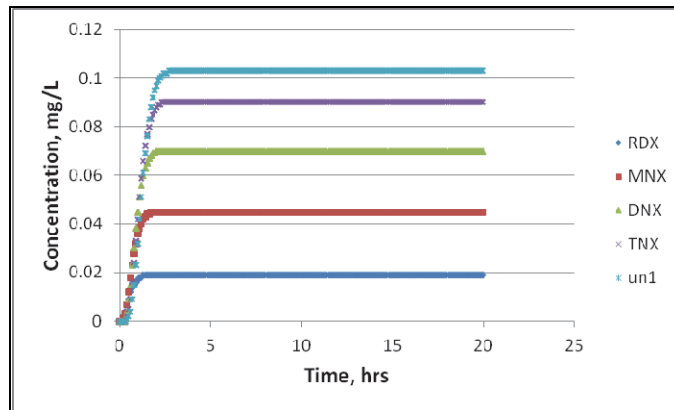


Figure 8. Concentrations of RDX and degradation products versus time at $X = 0.25$ m for hypothetical, longitudinal reactor test case.

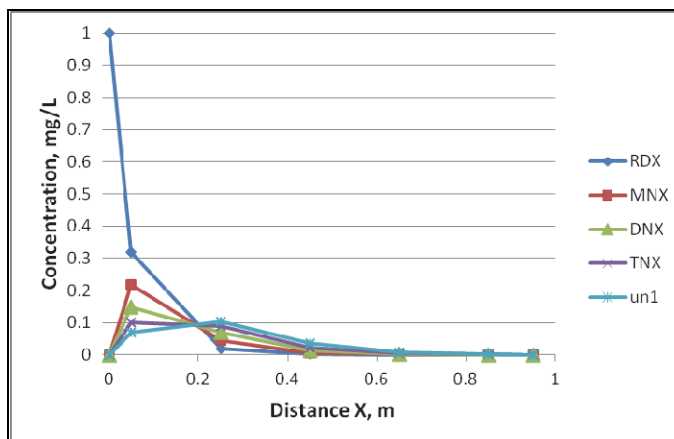


Figure 9. Concentrations of RDX and degradation products versus X after 20 hr for hypothetical, longitudinal reactor test case.

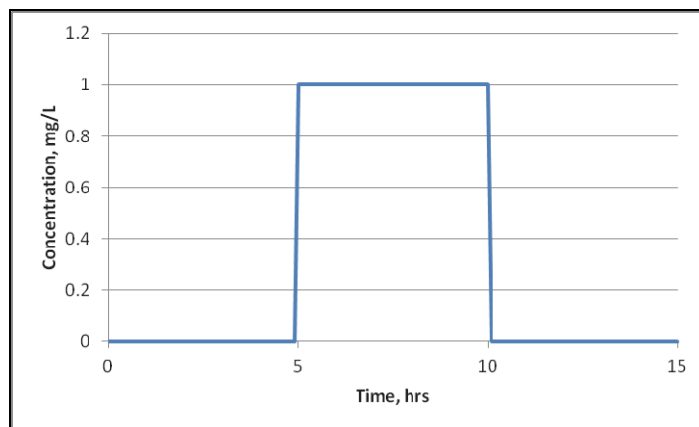


Figure 10. Input tracer pulse entering hypothetical longitudinal reactor.

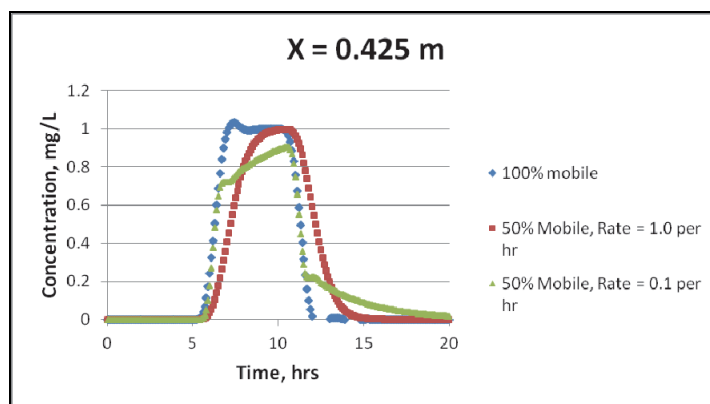


Figure 11. Tracer concentration versus time for tracer pulse in longitudinal reactor at location $X = 0.425$ m with 100% and 50% mobile domain.

The 1D, longitudinal reactor model was applied to meso-scale laboratory tests conducted in the ERDC Environmental Laboratory. The meso-scale reactor consisted of a 4-ft-long by 1-ft, 4-in.-high by 1-ft, 8-in.-wide chamber filled with a porous media consisting of gravel, cypress mulch, and iron filings. The porous media was saturated with water. Acetate was added to the system to specifically feed the iron-reducing organisms (Madigan et al. 2002) naturally occurring on the reactor packing. After the iron-reducing microbes established a reducing environment, dissolved RDX was introduced in the water influent, which had a constant flow rate of about 120 L/hr. The RDX concentration in the influent was relatively constant at about 0.77 mg/L. The chamber was baffled into four compartments where the flow moved vertically downward within the first compartment passing underneath the first baffle, and then the flow moved vertically upward in the second compartment before passing over the second baffle. Flow passed under the third baffle and then over the end wall as it exited the chamber. A sampling port was placed in each chamber compartment with the intake located 8 in. below the water surface. Thus, the first sampling port was 8 in. (0.2 m) from where the influent entered the chamber. Pore-water concentrations were measured at each sampling port.

Multiple laboratory tests were conducted with the meso-scale reactor using approximately the same test conditions. Multiple tests were run since it was difficult to maintain a constant flow and input RDX concentration. The results from tests 2, 3, and 4 were averaged to obtain a single influent RDX concentration and time-varying, observed RDX concentrations at the first sampling port. RDX was not detected at the other sampling ports. RDX degradation products were not measured. With a constant influent RDX loading rate and water flow rate, steady-state conditions should be reached eventually with the model.

The model inputs for the meso-scale laboratory reactor test are shown in Figure 12. The reactor length was set to 0.21 m or slightly greater than the distance to the first sampling port. Default values were used for the two kinetic reaction parameters. The only other uncertain inputs were the two parameters describing dual-domain mass transfer. These parameters were varied over multiple model runs, and model results were compared with the observed data for RDX at the first sampling port. It was determined that model results close to those observed could only be obtained for the fraction of mobile domain (f) set to 1.0. With any immobile domain, the computed steady-state RDX concentrations exceeded those observed by as much as double those observed in some cases. The reaction rate in the immobile domain is much less than for the mobile domain due to more limiting mass transfer. Dual-domain mass transfer may not be an appropriate mechanism for describing the flow within the reactor. It is possible that the flow can totally bypass some regions of the reactor without providing any opportunity for mass transfer from flowing water to dead-end pore spaces.

"Meso-scale application with 1D surface-site reactor m			
"Length, m"		0.21	
"Width, m"		.508	
"Height, m"		.305	
"Porosity"		0.50	
"fraction mobile"		1.	
"Dispersivity constant"		0.1	
"domain mass trans rate, 1/hr"		0.1	
"RDX mole. diffus., cm2/sec"		5.9E-6	
"packing solids diam, m"		.01	
"Fe mass in reactor, kg"		2.0	
"Fe half sat conc, k0, mol/L"		1.806	
"Fe max reac rate, kmax, 1/min"		2.824	
"RDX initial, mg/L"		0.0	
"number of delta x"		10	
"delta t, hr"		.002	
"simulation duration, hr"		2.0	
"DX output intervals"		1	
"solution scheme"		1	
"Time, hr	flowin, L/hr	RDX in, mg/L	Tracer in, mg/L"
0.0	120.0	.77	1.0
2.0	120.0	.77	1.0

Figure 12. Input parameters for longitudinal reactor model, meso-scale laboratory reactor test.

Model-computed RDX concentrations at $X = 0.2$ m for the inputs shown in Figure 12 are plotted versus time in Figure 13 along with observed RDX concentrations at that location. Again, this is for $f = 1.0$. The model compares quite well with the observations, even when using the default kinetic reaction parameters. Slight adjustments to these parameters can improve agreement with observed results.

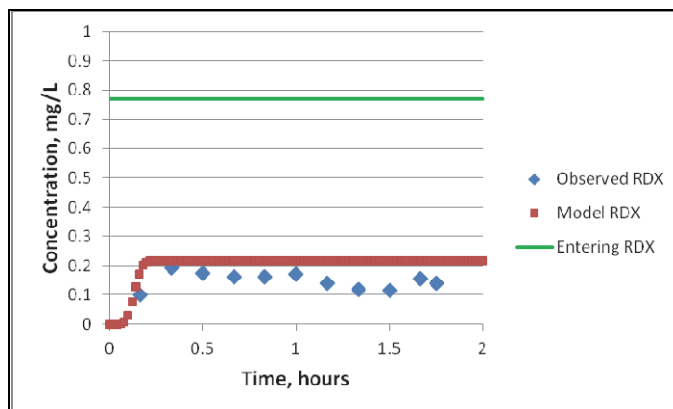


Figure 13. Concentrations of RDX versus time at X = 0.2 m for first sampling port of the meso-scale laboratory reactor.

CONCLUSIONS: This model formulation includes the coupling of mass transfer of dissolved constituents from pore water to iron solid surfaces and surface site reduction-reaction kinetics. Two model versions were developed, a batch reactor version, and a 1D, longitudinal reactor version. The latter version is far more versatile for simulating field conditions since it can handle time-varying influent loading and water flow rate. The good agreement between model results and meso-scale laboratory data indicates that the default kinetic reaction parameters may be applicable, and the use of dual-domain mass transfer may be inappropriate and not needed. Additional laboratory and/or field data are required to complete model testing, evaluation, and validation.

POINT OF CONTACT AND ACKNOWLEDGEMENT: For additional information, contact Dr. Mark Dortch (601) 634-3517, Mark.S.Dortch@usace.army.mil. This study was funded through the Green Range Program of the U.S. Army Environmental Quality Technology (EQT) Research Program by the U.S. Army Engineer Research and Development Center. This technical note should be cited as follows:

Dortch, M. S., and H. M. Smith. 2013. *Modeling RDX reduction within iron bed reactors*. EQT Technical Notes Collection. ERDC TN-EQT-13-1. Vicksburg, MS: US Army Engineer Research and Development Center.

REFERENCES

- Geller, J. T., and J. R. Hunt. 1993. Mass transfer from nonaqueous phase organic liquids in water-saturated porous media. *Water Resources Res.* 29(4): 833-845.
- Liu, G., C. Zheng, and S. M. Gorelick. 2007. Evaluation of the applicability of the dual-domain mass transfer model in porous media containing connected high-conductivity channels. *Water Resources Res.* 43(W12407):1-12.
- Madigan, M. T., J. M. Martinko, and J. Parker. 2002. *Brock biology of microorganisms*, 10th ed. Upper Saddle River, NJ: Prentice Hall, 588.
- Miyauchi, T. 1971. Film coefficients of mass transfer of dilute sphere-packed beds in low flow rate regime. *J. of Chem. Eng. of Japan* 4(3):34-41.

- Shrout, J. D., B. Sutton, L. Sherburne, P. Larese-Casanova, M. M. Scherer, G. F. Parkin, R. L. Valentine, C. L. Just, and P. J. J. Alvarez. 2004. *Fe(0)-based-bioremediation of RDX-contaminated groundwater*. 2003 Final Annual Report, Project number CU1231, prepared by Department of Civil and Environmental Engineering, University of Iowa for SERDP/ESTCP Program, Arlington, VA.
- Szecsody, J. E., J. S. Fruchter, M. A. McKinley, C. T. Resch, and T. J. Gilmore. 2001. *Feasibility of in-situ redox manipulation of subsurface sediments for RDX remediation at Pantex*. Report PNNL-13746. Richland, WA: Pacific Northwest National Laboratory.
- Wanaratna, P., C. Christodoulatos, and M. Sidhoum. 2006. Kinetics of RDX degradation by zero-valent iron (ZVI). *J. Hazardous Materials* 136:68-74.
- Wilson, E. J., and C. J. Geankoplis. 1966. Liquid mass transfer at very low Reynolds numbers in packed beds. *Ind. Eng. Chem. Fundam.* 5(1):9-14.
- Zheng, C., and P. Wang. 1999. MT3DMS: *A modular three-dimensional multispecies transport model for simulation of advection, dispersion, and chemical reactions of contaminants in groundwater systems: Documentation and user's guide*. Contract Report SERDP-99-01. Vicksburg, MS: U.S. Army Engineer Research and Development Center.

NOTE: The contents of this technical note are not to be used for advertising, publication or promotional purposes. Citation of trade names does not constitute an official endorsement or approval of the use of such products.